# The structure of a Staphylococcus aureus leucocidin component (LukF-PV) reveals the fold of the water-soluble species of a family of transmembrane pore-forming toxins

Jean-Denis Pedelacq, Laurent Maveyraud, Gilles Prévost, Lamine Baba-Moussa, Ana González, Emmanuel Courcelle, William Shepard, Henri Monteil, Jean-Pierre Samama, Lionel Mourey

# The structure of a *Staphylococcus aureus* leucocidin component (LukF-PV) reveals the fold of the water-soluble species of a family of transmembrane pore-forming toxins

Jean-Denis Pédelacq[1], Laurent Maveyraud[1], Gilles Prévost[2], Lamine Baba-Moussa[2], Ana González[3], Emmanuel Courcelle[1], William Shepard[4], Henri Monteil[2], Jean-Pierre Samama[1]* and Lionel Mourey[1]

**Background**: Leucocidins and γ-hemolysins are bi-component toxins secreted by *Staphylococcus aureus*. These toxins activate responses of specific cells and form lethal transmembrane pores. Their leucotoxic and hemolytic activities involve the sequential binding and the synergistic association of a class S and a class F component, which form hetero-oligomeric complexes. The components of each protein class are produced as non-associated, water-soluble proteins that undergo conformational changes and oligomerization after recognition of their cell targets.

**Results**: The crystal structure of the monomeric water-soluble form of the F component of Panton–Valentine leucocidin (LukF-PV) has been solved by the multiwavelength anomalous dispersion (MAD) method and refined at 2.0 Å resolution. The core of this three-domain protein is similar to that of α-hemolysin, but significant differences occur in regions that may be involved in the mechanism of pore formation. The glycine-rich stem, which undergoes a major rearrangement in this process, forms an additional domain in LukF-PV. The fold of this domain is similar to that of the neurotoxins and cardiotoxins from snake venom.

**Conclusions**: The structure analysis and a multiple sequence alignment of all toxic components, suggest that LukF-PV represents the fold of any water-soluble secreted protein in this family of transmembrane pore-forming toxins. The comparison of the structures of LukF-PV and α-hemolysin provides some insights into the mechanism of transmembrane pore formation for the bi-component toxins, which may diverge from that of the α-hemolysin heptamer.

Addresses: [1]Groupe de Cristallographie Biologique, Institut de Pharmacologie et de Biologie Structurale du CNRS, 205 route de Narbonne, 31077 Toulouse Cedex, France, [2]Laboratoire de Toxinologie et d'Antibiologie Bactériennes, Institut de Bactériologie de la Faculté de Médecine, Université Louis Pasteur, Hôpitaux Universitaires de Strasbourg, 3 rue Koeberlé, 67000 Strasbourg, France, [3]European Molecular Biology Laboratory, Hamburg Outstation, DESY, Notkestraße 85, Hamburg D-22603, Germany and [4]LURE, Université Paris-Sud, 91405 ORSAY Cedex, France.

*Corresponding author.
E-mail: samama@ipbs.fr

Key words: bi-component leucotoxins, crystal structure, LukF-PV, MAD, transmembrane pore

Received: 5 November 1998
Revisions requested: 4 December 1998
Revisions received: 18 December 1998
Accepted: 5 January 1999

Published: 26 February 1999

Structure March 1999, 7:277–287
http://biomednet.com/elecref/0969212600700277

 ISSN 0969-2126

## Introduction

Leucocidins (Luk) and γ-hemolysins (Hlg) are bi-component toxins secreted by *Staphylococcus intermedius* and *Staphylococcus aureus*, one of the most frequently isolated pathogens found in hospitals [1–6]. These toxins target polymorphonuclear cells, monocytes, macrophages and erythrocytes and comprise the family of staphylococcal bi-component leucotoxins [3,7]. Their toxicity involves the synergistic combination of a class S and a class F component [1], two non-associated exoproteins. These proteins undergo conformational changes and form oligomeric complexes after recognition of their cell targets, a process leading to transmembrane-pore formation [5,8] and, ultimately, to cell death.

Several Luk and Hlg toxins have been isolated from various *S. aureus* strains. The genes for most of these isolated toxins have been cloned and sequenced [2–4,6,9–11], and the corresponding proteins have been partitioned into the class F and class S subtypes. Among these toxins, the Panton–Valentine leucocidin (PVL) was the first to be reported [12], purified and characterized [1]. PVL-producing strains are associated with primary cutaneous lesions, particularly furuncles [13–15], and the PVL toxin was shown to be highly active on human and rabbit polymorphonuclear leucocytes [3,8]. This toxicity requires the interaction of the S component of PVL (LukS-PV) with a membrane-bound receptor on human polymorphonuclear neutrophils (PMNs), with a $K_D$ of less than 1 nM [16], followed by the binding of the F component of PVL (LukF-PV) [17,18]. It has been shown by flow cytometry, spectrofluorimetry and immunological studies that these sequential interactions at the membrane surface induce several responses of the target cells, and that pores, which are specific for the traffic of monovalent cations, are formed [8,19–21]. Biochemical data argued for a heterohexameric assembly of the bi-component toxins. Ultracentrifugation of toxins solubilized from erythrocyte membranes indicated a molecular weight in the order of 200 kDa and electrophoretic separations showed similar amounts of the F (MW 34 kDa) and S (MW 32 kDa)

components [5]. Studies of the interaction of several bi-component toxins with purely lipidic vesicles, indicated that they form membrane-attached oligomers. The two components of each toxin were present in equal amounts, suggesting a molar ratio of 1:1 in the oligomer [22]. The best fit of the statistical analysis of the kinetics of vesicle permeabilization indicated that the pores formed by the bi-component toxins were hexameric species [22].

Here, we report the three-dimensional X-ray structure of the secreted, water-soluble form of LukF-PV at 2.0 Å resolution. The multiwavelength anomalous dispersion (MAD) method was used to solve the structure of this 301 amino acid protein. The LukF-PV structure was compared with that of α-hemolysin from *S. aureus* [23], another pore-forming toxin [24], which has been described in its homoheptameric pore-forming state [25]. Our study shows the conservation of the core domains between these two toxins [26] and illustrates the fold of the stem domain prior to membrane insertion. The study also yields insights into some of the significant conformational changes pertaining to the mechanism of assembly in this family of toxins.

## Results and discussion

### Overall structure

The three-dimensional structure of LukF-PV contains 22 β strands (64.4%) and three short segments of either $3_{10}$ or α helices (5.3%). These secondary structure elements are organized into three structural domains: the β sandwich, the rim and the folded stem (Figure 1a). The β-sandwich domain (residues 1–61, 80–102, 154–169, 219–249 and 268–301) is made of two six-stranded antiparallel β sheets facing each other with an average angle of 30°. The rim domain (residues 62–79, 170–218 and 250–267) forms an antiparallel four-stranded open-face sandwich [27], topped by a stretch of residues (182–218). The conformation of this stretch may be described as two consecutive Ω loops followed by all the helical segments found in LukF-PV. The core of the protein, made of the β sandwich and rim domains, is similar to that of the α-hemolysin protomer (Protein Data Bank [PDB] code 7AHL) [23]. Superimposition of the two protein structures can be achieved using either the β-sandwich or the rim domains: the root mean square (rms) differences are 0.82 Å (for 116 Cα atoms) and 0.89 Å (for 74 Cα atoms), respectively. However, the respective orientations of the β-sandwich and rim domains differ in the two toxins (Figure 1b), due to a rigid-body displacement which can be described as a 10.7° rotation followed by a 0.19 Å translation along the rotation axis. This movement may be related to the large conformational change in the stem region of the proteins that occurs during the process of membrane insertion [28,29].

Sequence alignment of LukF-PV and α-hemolysin was performed, based on the superimposition of their three-dimensional structures. The alignment was then extended to all class F proteins, which share around 70% identity, and also to the class S proteins, which share 59–75% identity among one another. Between them, these two protein classes share 26–30% identity. The resulting multiple sequence alignment (Figure 2) revealed several conserved residues in α-hemolysin, class F and class S proteins. The positions of these residues, and their contribution to the protein fold, were analyzed using the LukF-PV three-dimensional structure. All of these residues have an important structural role and most could be associated into two groups. The first group comprises 12 residues: Ile59, Tyr82, Tyr99, Pro101, Tyr149, Leu153, Trp164, Leu216, Phe221, Pro223, Phe225 and Tyr245. The sidechains of these residues form a continuous hydrophobic patch involving all the strands in the β-sandwich domain (Figure 3a), except for the three N-terminal strands (S1, S2 and S3) and the two C-terminal strands (SG and SH), which are located on the same side of the β sandwich. The strands S2, S3 and S4 are, nevertheless, held together by hydrogen-bond interactions formed between the invariant Arg247, located in strand SF, and the mainchain oxygen atoms of residues 30 and 60 (which belong to the β turn between strands S2 and S3 and to S4, respectively). These features suggest conservation of the β-sandwich fold in all proteins. The second group of invariant residues is located at the bottom of the rim domain and comprises eight residues: Phe76, Trp78, Met192, Phe193, Phe207, Asp250, Tyr252 and Asn265. The sidechains of these residues provide a number of hydrophobic contacts, and polar interactions are exchanged between three buried residues (Figure 3b). The amide sidechain of Asn265 is at hydrogen-bonding distance from the nitrogen atom of the indole ring of Trp78 and from the carboxylic group of Asp250. The conservation of these residues and interactions might be regarded as a folding determinant of the rim domain. The formation of this core may be needed to accommodate the significant sequence variations between the class F and S proteins, which are prevalent in the two Ω-loop regions of the rim domain (Figure 2).

### Conformational changes between the initial monomeric water-soluble and final pore-forming states

The X-ray structures of LukF-PV and the self-assembling α-hemolysin homoheptamer illustrate the molecular species at the first and last steps of pore formation, respectively. Pore formation is commonly described as a four-step process involving the water-soluble secreted form, the membrane-bound monomer [30], an oligomeric pre-pore [31,32], and finally, the transmembrane pore itself [25]. The stem region, comprising residues 106–148, is also known as the glycine-rich stem. In each protomer of the α-hemolysin heptamer, the stem forms two 65 Å long antiparallel β strands, which protrude from the protein core (Figure 1b) and constitute one building unit of the membrane-spanning 14-stranded β barrel [23]. In the water-soluble LukF-PV protein, the stem region is folded as a third domain made of three

**Figure 1**

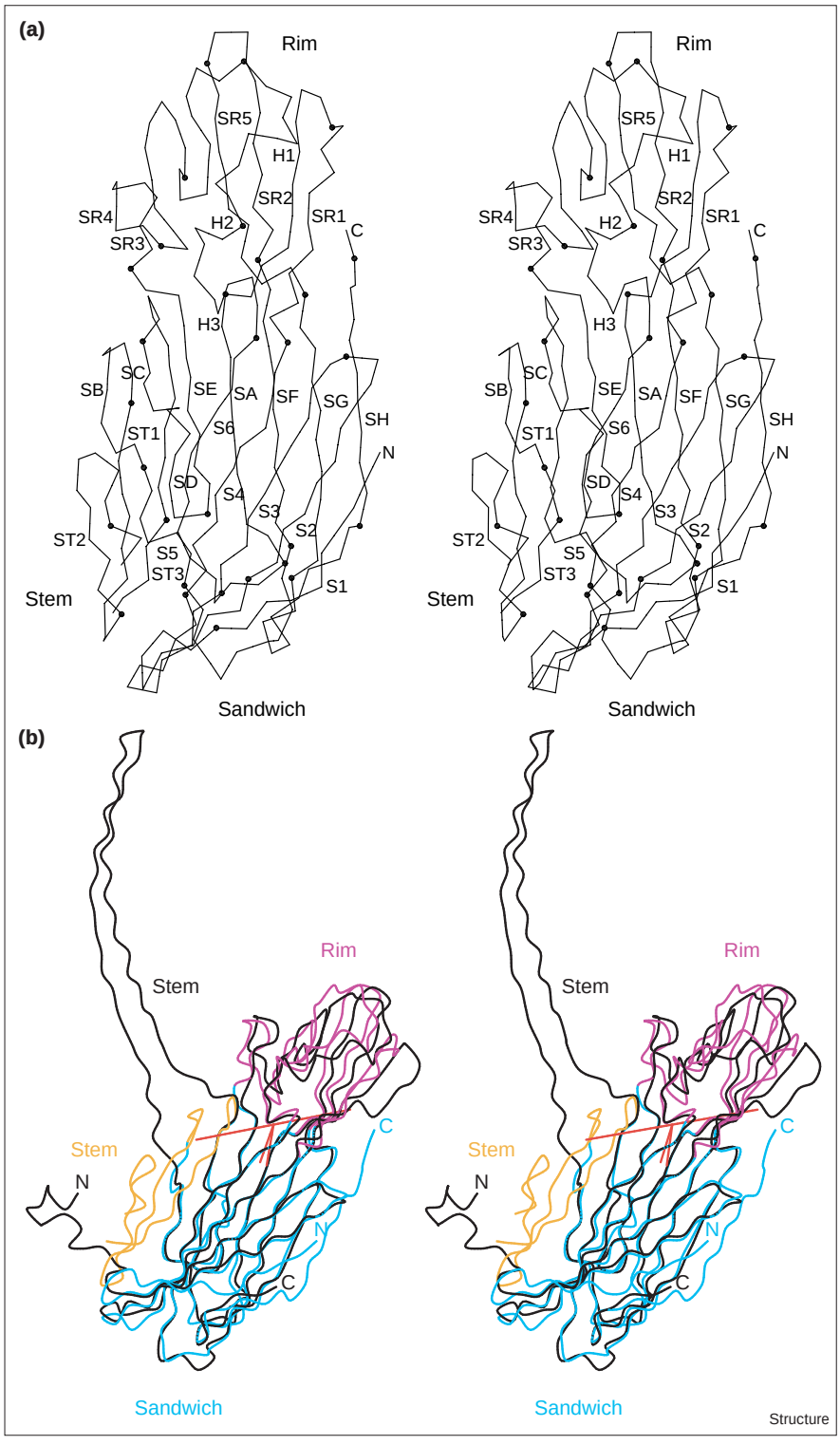


Structural domains in LukF-PV and α-hemolysin. **(a)** Stereoview Cα trace of LukF-PV. Every tenth Cα atom is indicated by a black dot. The N and C termini, the secondary structure elements and the three domains are labeled. **(b)** Stereoview of LukF-PV (the β-sandwich, rim and stem domains are shown in cyan, magenta and orange, respectively) superimposed onto one protomer of α-hemolysin in the heptameric oligomer (black). The rotation axis and the angular range describing the rigid-body motion (see text) are depicted in red. (The figure was produced using the program MOLSCRIPT [52].)

antiparallel β strands (ST1, ST2 and ST3) linked by one β turn and one right-handed cross-over connection (Figure 1). The junction to the β-sandwich domain is provided by two short antiparallel strands: SB (residues 103–105) and SC (residues 149–153). The stem domain is packed onto the β-sandwich core, excluding an area of 2750 Å$^2$ from

**Figure 2**

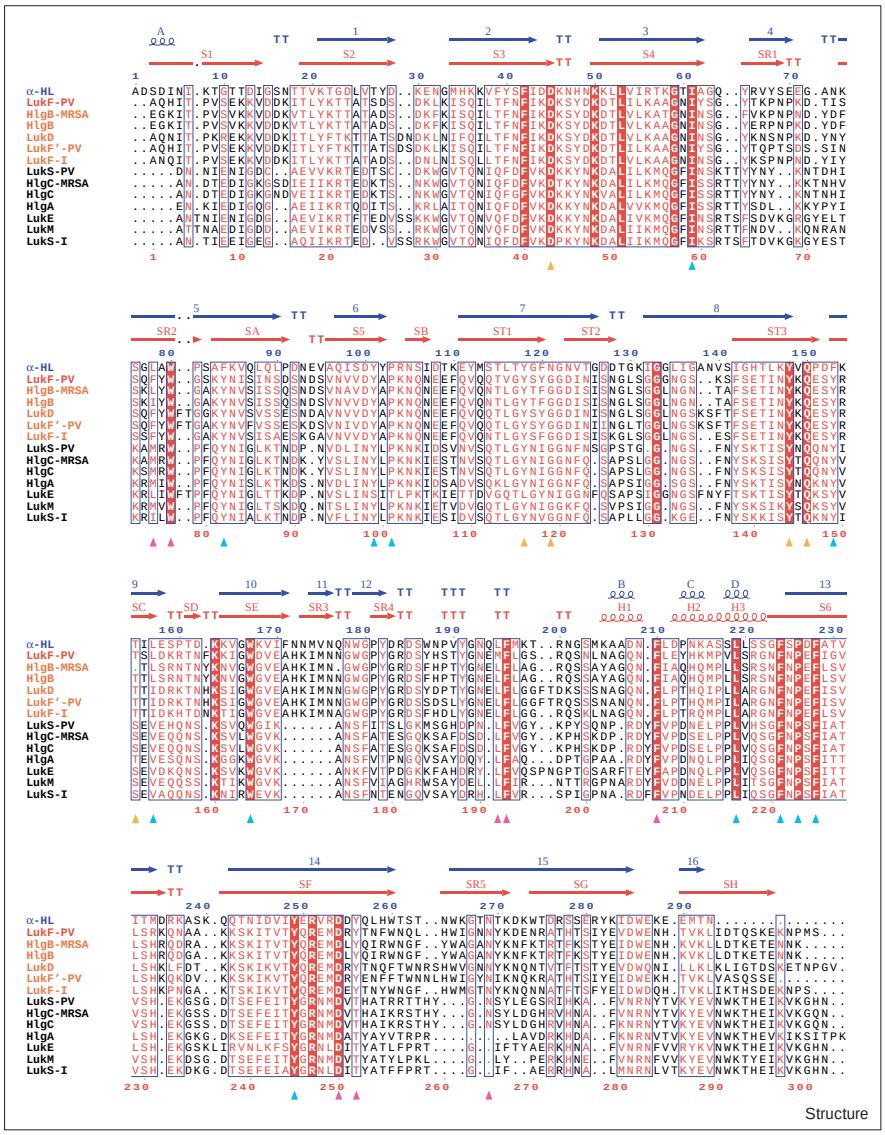


Sequence alignment for *Staphylococcus aureus* α-hemolysin (α-HL), *S. aureus* leucocidins (LukF-PV, LukD, LukF′-PV, LukS-PV, LukE and LukM), *Staphylococcus intermedius* leucocidins (LukF-I and LukS-I), and *S. aureus* γ-hemolysins (HlgB-MRSA, HlgB, HlgC-MRSA, HlgC and HlgA). The names of the F and S components of the bi-component toxins are written in orange and black, respectively. The alignment was based on the structure superimposition of LukF-PV and α-HL. Secondary structure elements of α-HL (blue) and LukF-PV (red) were assigned using the program DSSP [53]: β strands are shown as arrows and α helices as coils; TT and TTT are used to mark a β turn and an α turn, respectively. Sequence homologies are highlighted in red; sequence identities are shown as white letters on a red background. Invariant residues in the β sandwich, the rim and the stem domains are indicated using triangles with the same color code as in Figure 1b. The sequence numbering in blue is for α-HL and the numbering in red is for LukF-PV. (The figure was created using ESPript [http://www.ipbs.fr/ESPript].)

the solvent. At each side of the stem–β-sandwich interface, two groups of invariant residues provide a set of interactions, which suggests that the fold of the stem domain should be similar in all monomeric water-soluble α-hemolysin, class F and class S proteins (Figure 4). The sidechain of Asp43, from strand S3 of the β-sandwich domain, is located at hydrogen-bonding distance from both the mainchain nitrogen atom of residue Gly119 and the phenolic group of Tyr116 of the stem. These interactions would be impaired by the Cβ atom of any amino acid at position 120, and probably explains the invariance of Gly120 (Figure 2). At the other edge of this interface, hydrogen bonds are exchanged between Thr151 Oγ1 and the sidechain atoms of residues Tyr144 and Gln146 from the folded stem (Figure 4).

Pore formation by PVL requires the unfolding of the stem domain. The differences in solvent accessibility of the residues of this domain, in its folded and α-hemolysin-like extended conformation, were evaluated. This calculation indicated that the sidechains that will be oriented towards the nonpolar part of the lipid bilayer are, in most cases, involved in the stem–β-sandwich domain interface. A search for structural homology with other protein structures using the programs DALI [33] and DEJAVU [34] revealed significant similarity, despite very weak sequence homology, between the stem domain and two toxins isolated from snake venom: erabutoxin A [35] (PDB code 5EBX) and toxin-γ [36] (PDB code 1TGX). The molecular architecture of these two toxins is known as the three-finger fold [37]. The three central β strands, and loops II and III of these

**Figure 3**

Stereoview superimposition of the three-dimensional structures of LukF-PV (thick lines and black bonds) and α-hemolysin (thin lines and open bonds). The sidechains of the invariant residues forming the core of the domains are shown with atoms in standard colours. The superimposition of (a) the β-sandwich domains and (b) the rim domains. (The figure was produced using the program MOLSCRIPT [52].)

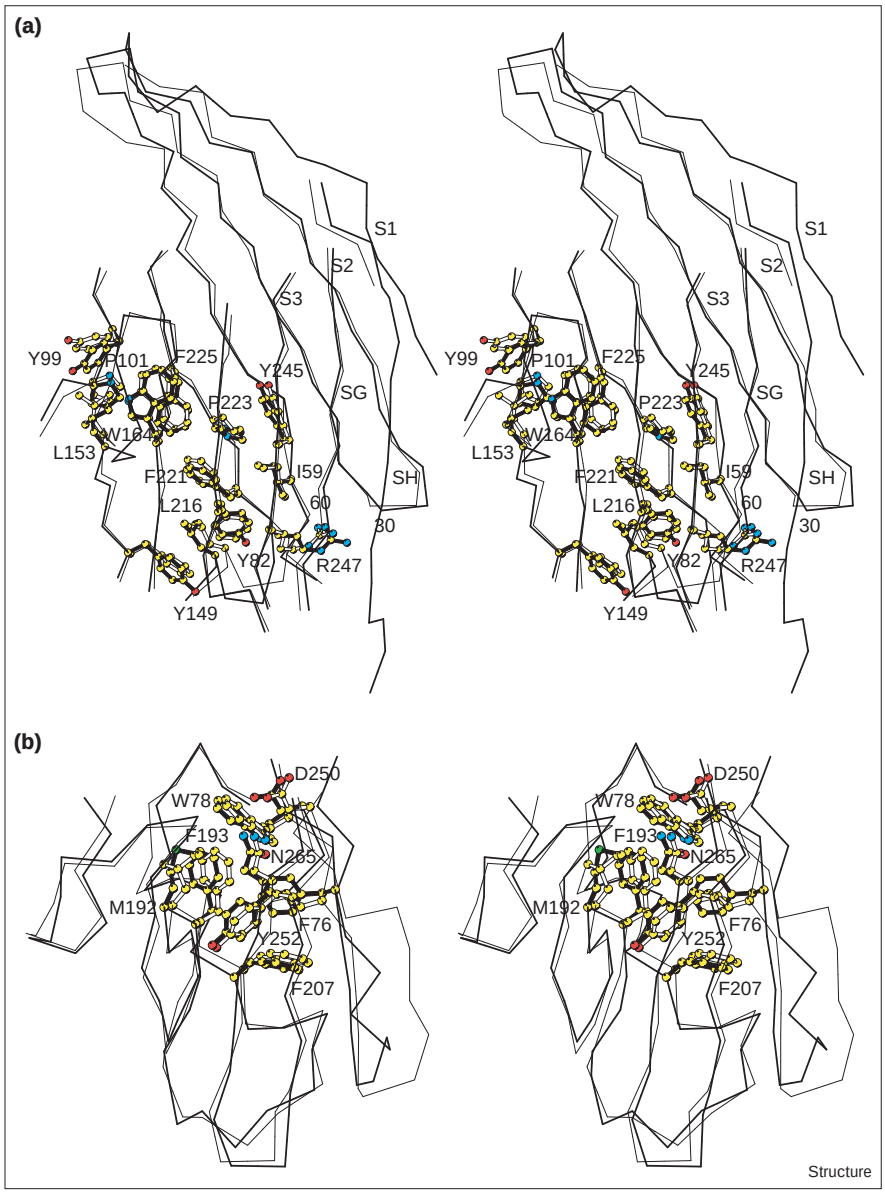


toxins (the conformation of which is constrained by four disulfide bridges) encompass the fold of the stem in LukF-PV (Figure 5). The possible functional significance of this structural similarity with respect to protein–membrane interactions remains to be documented for the *S. aureus* toxins. However, this finding suggested that formation of a disulfide bridge between residues 128 and 144 in LukF-PV, which would be analogous to the link between Cys43 and Cys54 in the snake venom toxins (Figure 5), may be envisioned. Such an engineered *S. aureus* toxin, where the unfolding process of the stem domain would not go to completion, may help to clarify some of the early steps of membrane pore formation.

The sequence alignment (Figure 2), and the structure superimposition of LukF-PV and the α-hemolysin protomer indicate the invariance, in both residue type and position, of Pro101 and Tyr149 (LukF-PV numbering), the two residues between which the very large conformational change of the stem region occurs. These hinge points interact with residues from the β-sandwich core. The mainchain carbonyl oxygen atoms of residues Ala100 and Pro101 form hydrogen-bond interactions to the mainchain nitrogen atom of Ile226 from strand S6, and the nitrogen atom of the indole ring of the invariant Trp164, respectively. In addition to the van der Waals contacts established by the aromatic ring, the phenolic hydroxyl group of

**Figure 4**

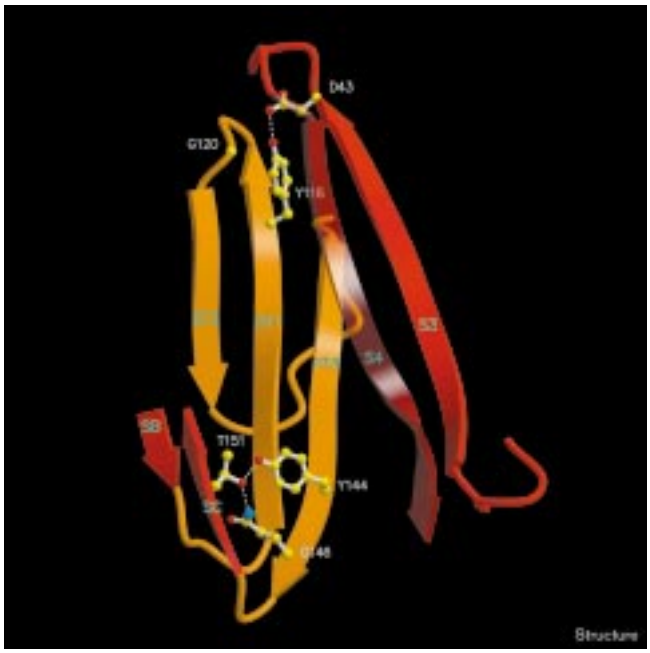


Ribbon representation illustrating the interactions between invariant residues (see text) that anchor the folded stem domain (orange) to the β-sandwich domain (red). (The figure was produced using the program MOLSCRIPT [52].)

Tyr149 is at hydrogen-bonding distance (2.6 Å) from the mainchain oxygen atom of Gly79 and the hydroxyl group of Ser217. These interactions may have an important role in preserving the positions of Pro101 and Tyr149 during the structural transition leading to the disruption of the stem–β-sandwich domain interface and the unfolding of the stem. The free energy associated with these events might be provided by the protein monomer–membrane interactions prior to oligomerization and pore formation [38].

### Homo-oligomers, hetero-oligomers and protomer multiplicity

A significant structural difference was observed in the N-terminal regions of LukF-PV and the α-hemolysin protomer (Figure 1b). The difference in conformation, and the contribution of these 16 residues to protomer–protomer associations may be relevant to the final oligomeric state of these toxins.

The N-terminal region in LukF-PV, which is two residues shorter in all class F proteins compared to α-hemolysin, showed no sensitivity to proteolytic enzymes and constitutes the outermost external, 12-residue long strand (S1) of the β-sandwich domain (Figure 1a). In contrast, the N-terminal latch (residues 1–16) in α-hemolysin has no defined secondary structure. In the heptameric toxin, this region forms numerous interactions with adjacent protomers which contribute to the stability of the macromolecular assembly [23]. These interactions seem essential as deletion of only the two N-terminal residues abolishes the hemolytic activity of the toxin [30]. In the monomeric and soluble α-hemolysin, this region was found sensitive to proteolysis and assumed to be loosely organized [39].

In the process of α-hemolysin oligomerization, a cooperative effect between a conformational change of the N-terminal

**Figure 5**

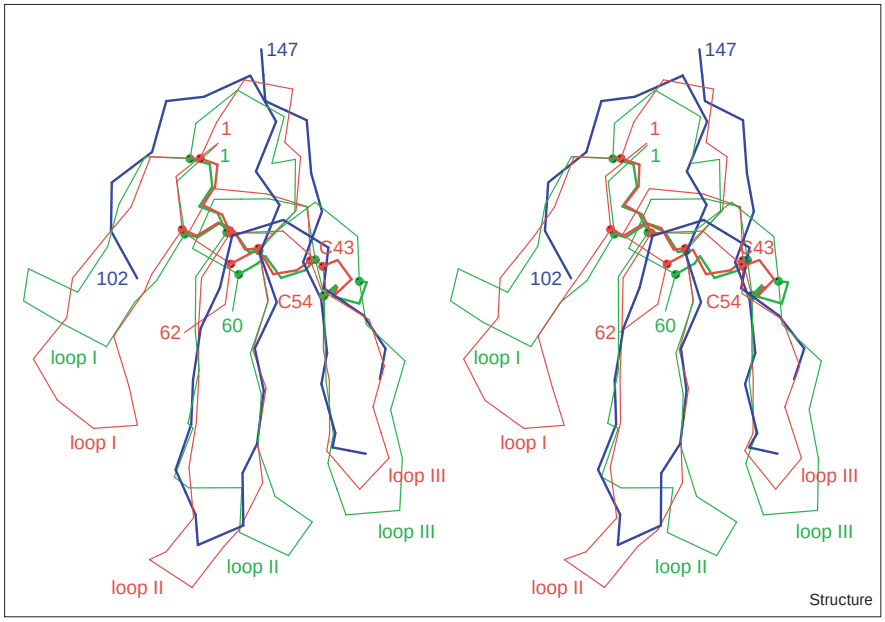


Stereoview of the stem domain of LukF-PV (deep blue) superimposed on the three-dimensional structures of erabutoxin A from *Laticauda semifasciata* (red) and toxin-γ from *Naja nigricollis* (green); the root mean square (rms) differences for 24 Cα atoms are 0.9 Å and 1.8 Å, respectively. The four disulfide bridges present in both snake venom toxins are displayed with thick lines and the Cα atoms of each cysteine residue are indicated by colored dots. (The figure was produced using the program MOLSCRIPT [52].)

region and the transition from the soluble monomeric form to the pore-forming heptameric structure was proposed [39]. The loose organization postulated for this region, and the inspection of the superimposed LukF-PV and α-hemolysin structures support this hypothesis. Accommodation of the 16 N-terminal residues, in the conformation they adopt in the pore-forming heptamer, seems sterically incompatible with a folded stem according to the LukF-PV structure (Figure 1b).

A similar oligomerization process for the bi-component toxins would imply that the N-terminal strand S1 dissociates from its antiparallel strand S2. Assuming that this transition occurs, the possibility that the F and S components may form homo- or heteroheptameric pores similar to that of α-hemolysin was examined. The α-hemolysin-like pore-forming protomers of the F and S proteins were generated with the reasonable assumption that the conformation of the unfolded stem regions should be very similar in all three proteins. The oligomers were modeled by superimposition of the unfolded stem regions of the F and S proteins onto each pair of strands of the 14-stranded β-barrel pore. Examination of the protomer–protomer contacts in these hypothetical heptamers showed that their formation was unlikely without additional conformational changes in the β-sandwich domain. A majority of seemingly incompatible sidechain substitutions, from α-hemolysin to the F and S proteins, occur for the residues involved in the 29 tight hydrogen-bond interactions contributing to the association of consecutive protomers in α-hemolysin. On the other hand, assuming unfolding of the stem domain but no dissociation of the N-terminal S1 strand from the β sandwich was also incompatible with the formation of heptameric oligomers of F and S proteins. Obvious steric clashes occur between adjacent protomers, which arise from the folded N-terminal strand. These modeling approaches suggested that the structure of the pore in PVL may diverge from the α-hemolysin heptamer, which would agree with the proposal that the oligomeric bi-component toxins contained equimolar proportions of class F and S monomers in a hexameric assembly [5,22].

The transmembrane pore resulting from a hexameric assembly would be a 12-stranded antiparallel β barrel, the geometrical and topological characteristics of which have been described [40,41]. In this barrel, the shear number (S) equals the number of strands in the β sheet, a feature that was also specific to the 14-stranded β barrel α-hemolysin pore. The inner diameter of the pore (21 Å) is in good agreement with the experimental data on γ-hemolysin [5] and PVL [42], which indicated a functional diameter of about 21–24 Å. The tilt of the strands to the β barrel axis is 37°, in line with the average angle formed by the β strands with the normal of the plane of the membrane, which was estimated to be 36–38° for the bi-component toxins in small unilamellar vesicles [22]. The heterohexameric pore was constructed assuming unfolded stem regions for the F and S proteins and without altering the position of strand S1. Each antiparallel β strand of the stem was superimposed onto one pair of strands of the 12-stranded β barrel, and the resulting positions of the β-sandwich and rim domains in the mushroom-shaped complex showed no bad contacts (Figure 6). One of the

**Figure 6**

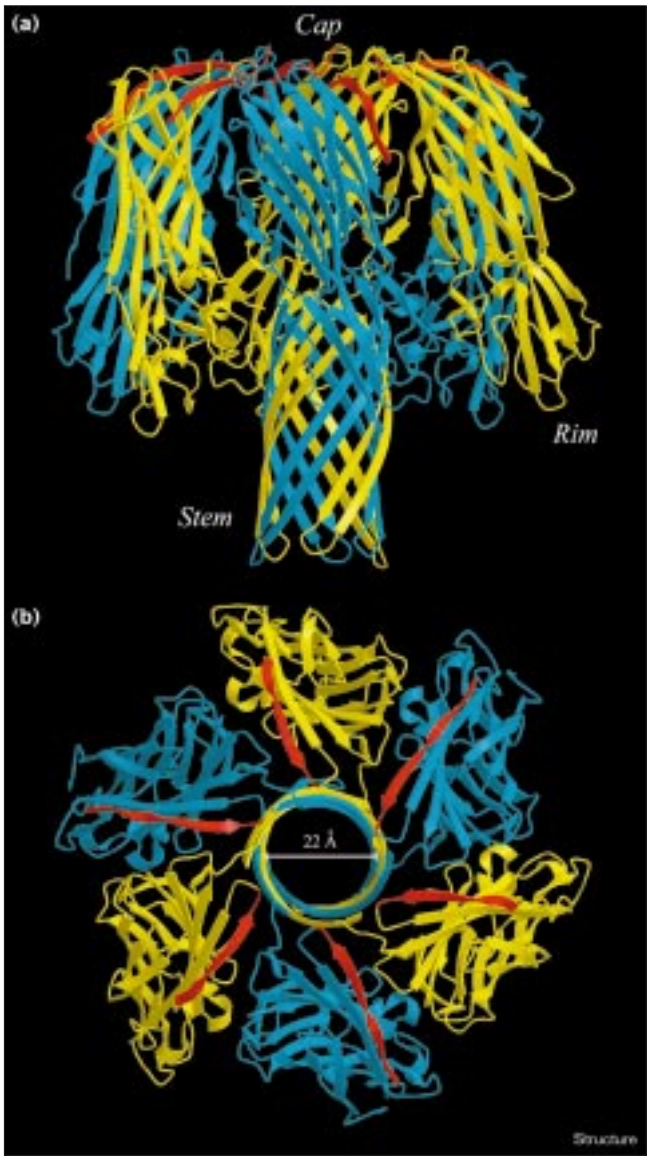


Molecular model of heterohexameric PVL assuming no unfolding of strand S1 from the β-sandwich domain. The conformation of the stem region was derived from that of the α-hemolysin protomer [23]. The architecture of the pore was based on the topology of a 12-stranded β barrel [41]. (a) View perpendicular to the sixfold axis. The LukF and LukS subunits are shown in blue and yellow, respectively; the N termini are shown in red. (b) View down the sixfold axis from the top of the cap. (The figure was produced using the program MOLSCRIPT [52].)

interprotomer interactions involved the folded N-terminal strand and the model suggested that additional residues at the N terminus should not impair oligomerization. We therefore engineered a LukF-PV protein containing eight additional residues (Gly-Pro-Leu-Gly-Ser-Pro-Glu-Phe) at the N terminus and found no change in the toxicity of this PVL on PMN cells compared to that of the native protein (GP, unpublished data).

Leucotoxins composed of a given S component and supplied with different class F proteins exhibit different levels of toxicity on selected cell types [11], suggesting either interaction of the F proteins with the membrane-bound receptor of LukS-PV or incomplete pore formation resulting from some mismatch between some F proteins, the S protein and/or the membrane components. The possible mismatch between the F and S proteins could only be addressed from the X-ray structure of LukF-PV. An analysis of the sequence variation within the class F proteins showed that they occur in regions located at the F–S interface, and at the solvent-exposed region of the toxin. The former location may be consistent with the different levels of cytotoxicity observed with the various combinations of S and F molecular species.

The protein monomer–membrane interactions are likely to contribute to the drastic conformational transitions leading to the disruption of the 2750 $Å^2$ interface between the folded stem and the β-sandwich domain, and to the formation of significant protomer–protomer interfaces in the oligomeric species [23]. These processes might be influenced by the chemical content of the membrane, which may provide some explanation for the recently proposed polymorphism of the α-hemolysin toxin formed in different membrane layers [43]. In the case of PVL, the binding of LukS-PV to its high-affinity membrane-bound receptor may also drive molecular events. The cooperative effect in the transition from a folded stem to other species, which in the case of the self-assembling α-hemolysin could involve the conformational change of the N-terminal region, may arise in PVL from protein–receptor binding interactions. The structure of the soluble form of LukF-PV should help in the design of engineered proteins for further investigations of the binding and oligomerization of these protein subunits in membranes.

## Biological implications

Leucocidins, γ-hemolysins and α-hemolysin are exotoxins produced by *Staphylococcus aureus*, a common pathogen in hospitals. These toxins are secreted as water-soluble proteins of about 33 kDa but form oligomeric species upon binding to the cell membrane. This oligomerization leads to pore formation and is commonly described as a four-step process involving the water-soluble species, the membrane-bound monomer, an oligomeric pre-pore and finally the transmembrane pore.

Although α-hemolysin is a self-assembling toxin, leucocidins and γ-hemolysins are bi-component toxins that act through the sequential binding and synergistic association of a class S and a class F component to form hetero-oligomeric complexes. X-ray structure determination of the pore-forming oligomer of α-hemolysin, formed in deoxycholate micelles, revealed a heptameric organization. In this mushroom-shaped structure, the transmembrane pore appears as a 14-stranded antiparallel β barrel in which each protomer contributes two 65 Å long antiparallel strands. In this work, the X-ray structure of the water-soluble form of the F component of the Panton–Valentine leucocidin (LukF-PV), solved by the multiwavelength anomalous dispersion (MAD) method, illustrates the molecular species that undergoes the conformational changes and oligomerization promoted by membrane association. The conservation of the folding determinants of the protein, established on the basis of a multiple sequence alignment of all toxic components, suggests that the structure of LukF-PV represents the fold of any water-soluble protein in this family of toxins. The membrane-spanning region of the toxin forms an additional domain in the monomeric protein, tightly packed onto the protein core. The topology of this domain is similar to that of erabutoxin A and toxin-γ from snake venom.

Biochemical and biophysical studies argued for hexameric assemblies of leucocidins and α-hemolysins, containing similar amounts of the F and S components. Modeling attempts of heptameric and hexameric oligomers of PVL, based on 14-stranded and 12-stranded antiparallel β-barrel pores, respectively, were in favor of the hetero-hexameric assembly of PVL.

## Materials and methods

### *Purification of LukF-PV*

The reference *S. aureus* ATCC49775 was grown in yeast extract casaminoacid sodium pyruvate (YCP) medium [11] for 16 h at 37°C with vigorous shaking. The proteins in the culture supernatant were precipitated with ammonium sulfate. The pellet was solubilized in 30 mM sodium phosphate (pH 6.5) and then dialyzed against the same buffer. Negatively charged proteins were discarded by two consecutive separations on SP fast flow and MonoS columns (Pharmacia, Uppsala, Sweden) using fast protein liquid chromatography (FPLC) at 4°C with an NaCl gradient ranging from 0 to 700 mM. Protein fractions (80–120 mM NaCl) were pooled and adjusted to 50 mM potassium phosphate, 1.5 M $(NH_4)_2SO_4$ (pH 7.0) for chromatography on an alkyl-superose FPLC column (Pharmacia). Pure LukF-PV was eluted from a linear $(NH_4)_2SO_4$ gradient (1.5–0 M). The protein was stored at 0.6 mg/ml ($OD_{280nm}$ = 1.0) in 30 mM sodium phosphate, 200 mM NaCl (pH 6.5).

### *Crystallization*

Crystals of LukF-PV were obtained at 4°C by seeding microcrystals in pre-equilibrated hanging drops containing the protein (20 mg/ml) in 200 mM Tris and MES buffer (pH 6.8–7.0), 21% PEG 4000 (W/V) and 7 mM cadmium chloride. The crystals belong to orthorhombic space group $P2_12_12_1$ with cell parameters a = 50.7 Å, b = 73.3 Å, c = 99.7 Å, with one molecule per asymmetric unit.

**Table 1**

**Data collection statistics.**

| Wavelength (Å) | Resolution (Å) (outer shell)* | Reflections measured/unique | Completeness (%) (outer shell)* | $R_{sym}$† (outer shell)* | $R_{iso}$‡ | $R_{ano}$§ |
|---|---|---|---|---|---|---|
| Remote $\lambda_1$ 1.1270 | 24.4–2.0 (2.12–2.0) | 96,992/21,089 | 85.0 (88.0) | 0.060 (0.101) | – | 0.037 |
| Edge $\lambda_2$ 1.1053 | 24.4–2.0 (2.12–2.0) | 92,737/21,121 | 85.1 (89.8) | 0.071 (0.123) | 0.042 | 0.048 |
| Peak $\lambda_3$ 1.1048 | 24.4–2.0 (2.12–2.0) | 80,455/21,495 | 86.7 (89.7) | 0.064 (0.111) | 0.040 | 0.056 |
| Remote $\lambda_4$ 0.8269 | 24.4–2.0 (2.12–2.0) | 74,044/20,710 | 83.3 (89.8) | 0.063 (0.121) | 0.051 | 0.050 |

*Values in parentheses are for the highest resolution shell. †$R_{sym} = \Sigma\Sigma | <I> - I_i | / \Sigma\Sigma I_i$. ‡$R_{iso} = \Sigma | F_{PH} - F_P | / \Sigma | F_P |$. §$R_{ano} = \Sigma | <I^+> - <I^-> | / \Sigma (<I^+> + <I^->)$.

### *Data collection and phasing*

A MAD experiment was performed on a single crystal soaked with $(NH_4)_2IrCl_6$. Soaking was performed in an X-ray capillary by adding the iridium salt solubilized in the reservoir solution to the crystal in mother liquor. The final concentration and soaking time were 2 mM and 16 h, respectively. An equal volume of a cryoprotectant solution (20% glycerol [w/v] in the solution used for heavy-atom soaking) was then added for 1 h. The content of the capillary was transferred on a glass plate and the crystal mounted in a cryo-loop and flash-cooled to 100K in a stream of nitrogen gas. Care was taken to properly orient the crystal in the cryo-loop in order to record the Bijvoet pairs on the same frame. MAD diffraction data were collected at four wavelengths on X31 beam line of the EMBL Hamburg Outstation at the Deutsches Elektronen-Synchrotron (DESY, Germany). A fluorescence spectrum, recorded with the frozen crystal prior to data collection, was used to select the wavelengths in the iridium $L_{III}$ absorption edge ($\lambda_2$ = 1.1053 Å, maximum of $|f'|$), at the peak ($\lambda_3$ = 1.1048 Å, maximum of $f''$) and at two remote wavelengths ($\lambda_1$ = 1.1270 Å and $\lambda_4$ = 0.8269 Å) (Figure 7). Data were collected on an 18 cm MAR research image plate with detector distance 180 mm, frame size 1° and approximately 4 min exposure time. Reflection intensities were processed using the program DENZO [44]. The CCP4 suite of programs [45] was then used to merge and scale these intensities and to compute the structure-factor amplitudes (Table 1). For scaling and all subsequent steps, the low-energy reference data set ($\lambda_1$) was chosen as 'native' data set. Three major heavy-atom sites were identified in dispersive difference Patterson maps at 4.0 Å resolution. Heavy-atom refinement and MAD phasing were conducted with SHARP [46] using all data between 24.4 and 2.0 Å (Table 2), which indicated four additional sites in the anomalous residual map computed at $\lambda_3$. The electron-density map was improved by solvent flattening in SOLOMON [47] assuming a solvent content of 48% in the unit cell.

### *Model building and crystallographic refinement*

The modified 2.0 Å resolution electron-density map allowed tracing of 88% of the LukF-PV molecule, including 81% of sidechain atoms. The structure was refined by the maximum-likelihood method as implemented in REFMAC [48] including a bulk-solvent correction computed in X-PLOR [49], followed by manual fitting into SIGMAA-weighted electron-density maps with TURBO-FRODO [50]. Reflections between 24.4 and 2.0 Å were used in the refinement, excluding a random set of data (5%) for the calculation of the free R factor [51]. The final model comprises 2389 nonhydrogen atoms in LukF-PV, seven iridium species, one cadmium ion, 168 water and 2 MES buffer molecules. The rms deviations from ideal geometry were calculated: bond lengths, 0.012 Å; angles, 2.3°; dihedrals, 27.7°. The crystallographic R value and $R_{free}$ were 0.20 (for 19,969 reflections) and 0.24 (for 1080 reflections), respectively. The average B factors are 15.3 Å$^2$ for protein atoms (14.2 Å$^2$ and 16.3 Å$^2$ for mainchains and sidechains, respectively), 50.9 Å$^2$ for the iridium species, 39.1 Å$^2$ for the cadmium ion and 31.5 Å$^2$ and 19.8 Å$^2$ for the MES buffer and water molecules, respectively. Ser129 and the three consecutive glycine residues (Gly130–Gly132) display the highest temperature factors in the structure and no clear electron density could be assigned to Asn133, Gly134 and Ser135. Flexibility of the polypeptide chain, rather than cleavage in this region, should be invoked as sodium dodecylsulfate polyacrylamide gel electrophoresis (SDS–PAGE) of dissolved crystals only revealed a single protein band corresponding to the full-length protein.

**Table 2**

**MAD phasing statistics.**

| Wavelength (Å) | $f'/f''$*(e$^-$) | $P_p^{iso}$† acentric/centric | $P_p^{ano}$† | $R_{Cullis}^{iso}$† acentric/centric | $R_{Cullis}^{ano}$† | FOM† acentric/centric |
|---|---|---|---|---|---|---|
| Remote $\lambda_1$ 1.1270 | –10.7/4.0 | – | 1.39 | – | 0.86 | 0.56/0.41 |
| Edge $\lambda_2$ 1.1053 | –22.0/8.5 | 1.84/1.18 | 2.06 | 0.57/0.59 | 0.72 | |
| Peak $\lambda_3$ 1.1060 | –16.8/15.5 | 1.01/0.78 | 2.46 | 0.61/0.63 | 0.63 | |
| Remote $\lambda_4$ 0.8269 | –3.8/10.2 | 1.29/0.97 | 1.81 | 0.71/0.75 | 0.76 | |

*Values of anomalous scattering factors, as refined by SHARP [46], used for phasing. †Phasing statistics provided by the program SHARP [46]; FOM, figure of merit.

**Figure 7**

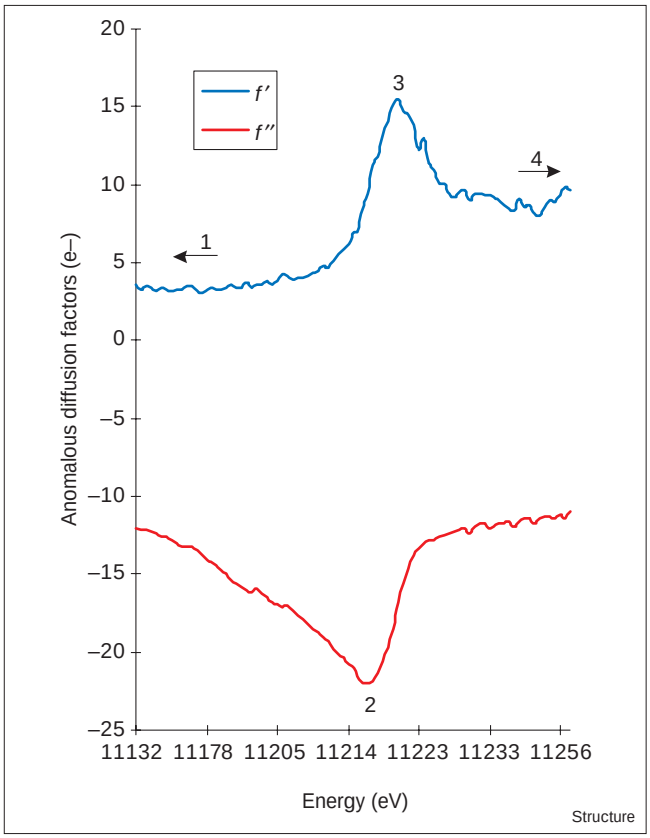


The energy dependence of the anomalous scattering factors *f′* and *f″* in the vicinity of the iridium $L_{III}$ absorption edge, as derived from the fluorescence spectrum. The energies corresponding to the four working wavelengths are labeled: 2 (edge), 3 (peak), 1 and 4 (two remote points).

### *Accession numbers*

The coordinates and structure factors are deposited in the Protein Data Bank with accession code 1pvl, to become available at the time of publication.

## Acknowledgements

We are grateful to the skillful technical assistance of D Keller for the purification of LukF-PV. We thank É de La Fortelle and G Bricogne for providing the SHARP program and for precious advice, P Gouet for his helpful assistance in the use of the program ESPript, MS Sansom and ID Kerr for kindly providing the coordinates of canonical β barrels and M Welch for his critical reading of the manuscript. This work was supported in part by the Direction de la Recherche et des Etudes Doctorales (grant EA 1318) and by the Région Midi-Pyrénées.

## References

1. Woodin, A.M. (1960). Purification of the two components of leucocidin from *Staphylococcus aureus*. *Biochem. J.* 75, 158-165.
2. Cooney, J., Kienle, Z., Foster, T.J. & O'Toole, P.W. (1993). The gamma-hemolysin locus of *Staphylococcus aureus* comprises three linked genes, two of which are identical to the genes for the F and S components of leukocidin. *Infect. Immun.* 61, 768-771.
3. Prévost, G., *et al.*, & Piémont, Y. (1995). Panton-Valentine leucocidin and gamma-hemolysin from *Staphylococcus aureus* ATCC 49775 are encoded by distinct genetic loci and have different biological activities. *Infect. Immun.* 63, 4121-4129.
4. Prévost, G., Bouakham, T., Piémont, Y. & Monteil, H. (1995). Characterisation of a synergohymenotropic toxin produced by *Staphylococcus intermedius*. *FEBS Lett.* 376, 135-140.
5. Sugawara, N., Tomita, T. & Kamio, Y. (1997). Assembly of *Staphylococcus aureus* γ-hemolysin into a pore-forming ring-shaped complex on the surface of human erythrocytes. *FEBS Lett.* 410, 333-337.
6. Kaneko, J., Muramoto, K. & Kamio, Y. (1997). Gene of LukF-PV-like component of Panton-Valentine leukocidin in *Staphylococcus aureus* P83 is linked with lukM. *Biosci. Biotech. Biochem.* 61, 541-544.
7. Tomita, T. & Kamio, Y. (1997). Molecular biology of the pore-forming cytolysins from *Staphylococcus aureus*, α- and γ-hemolysins and leukocidin. *Biosci. Biotech. Biochem.* 61, 565-572.
8. Finck-Barbançon, V., Duportail, G., Meunier, O. & Colin, D.A. (1993). Pore formation by a two-component leukocidin from *Staphylococcus aureus* within the membrane of human polymorphonuclear leukocytes. *Biochim. Biophys. Acta* 1182, 275-282.
9. Rahman, A., Izaki, K. & Kamio, Y. (1993). Gamma-hemolysin genes in the same family with lukF and lukS genes in methicillin resistant *Staphylococcus aureus*. *Biosci. Biotech. Biochem.* 57, 1234-1236.
10. Supersac, G., Prévost, G. & Piémont, Y. (1993). Sequencing of leucocidin R from *Staphylococcus aureus* P83 suggests that staphylococcal leucocidins and gamma-hemolysin are members of a single, two-component family of toxins. *Infect. Immun.* 61, 580-587.
11. Gravet, A., Colin, D.A., Keller, D., Girardot, R., Monteil, H. & Prévost, G. (1998). Characterization of a novel member, LukE-LukD, of the bi-component staphylococcal leucotoxins family. *FEBS Lett.* 436, 202-208.
12. Panton, P.N. & Valentine, F.C.O. (1932). Staphylococcal toxin. *Lancet* 222, 506-508.
13. Finck-Barbançon, V., Prévost, G. & Piémont, Y. (1991). Improved purification of leukocidin from *Staphylococcus aureus* and toxin distribution among hospital strains. *Res. Microbiol.* 142, 75-85.
14. Cribier, B., Prévost, G., Couppié, P., Finck-Barbançon, V., Grosshans, E. & Piémont, Y. (1992). *Staphylococcus aureus* leukocidin: a new virulence factor in cutaneous infections? An epidemiological and experimental study. *Dermatology* 185, 175-180.
15. Couppié, P., Cribier, B. & Prévost, G. (1994). Leukocidin from *Staphylococcus aureus* and cutaneous infections: an epidemiologic study. *Arch. Dermatol.* 130, 1208-1209.
16. Colin, D.A., Mazurier, I., Sire, S. & Finck-Barbançon, V. (1994). Interaction of the two components of leukocidin from *Staphylococcus aureus* with human polymorphonuclear leukocyte membranes: sequential binding and subsequent activation. *Infect. Immun.* 62, 3184-3188.
17. Woodin, A.M. & Wieneke, A.A. (1968). The cation-sensitive phosphatases of the leucocyte cell membrane. *Biochem. Biophys. Res. Commun.* 33, 558-562.
18. Noda, M., Kato, I., Matsuda, F. & Hirayama, T. (1981). Mode of action of staphylococcal leucocidin: relationship between binding of $^{125}$I-labeled S and F components of leucocidin to rabbit polymorphonuclear leukocytes and leucocidin activity. *Infect. Immun.* 34, 362-367.
19. Meunier, O., Falkenrodt, A., Monteil, H. & Colin, D.A. (1995). Application of flow cytometry in toxinology: pathophysiology of human polymorphonuclear leukocytes damaged by a pore-forming toxin from *Staphylococcus aureus*. *Cytometry* 21, 241-247.
20. König, B., Prévost, G., Piémont, Y. & König, W. (1995). Effects of *Staphylococcus aureus* leukocidins on inflammatory mediator release from human granulocytes. *J. Infect. Dis.* 171, 607-613.
21. Staali, L., Monteil, H. & Colin, D.A. (1998). The staphylococcal pore-forming leukotoxins open $Ca^{2+}$ channels in the membrane of human polymorphonuclear neutrophils. *J. Membr. Biol.* 162, 209-216.
22. Ferreras, M., Höper, F., Serra, M.D., Colin, D.A., Prévost, G. & Menestrina, G. (1998). The interaction of *Staphylococcus aureus* bi-component γ-hemolysins and leucocidins with cells and lipid membranes. *Biochim. Biophys. Acta* 1414, 108-126.
23. Song, L., Hobaugh, M.R., Shustak, C., Cheley, S., Bayley, H. & Gouaux, J.E. (1996). Structure of staphylococcal α-hemolysin, a heptameric transmembrane pore. *Science* 274, 1859-1866.
24. Füssle, R., Bhakdi, S., Sziegoleit, A., Tranum-Jensen, J., Kranz, T. & Wellensiek, H.J. (1981). On the mechanism of membrane damage by *Staphylococcus aureus* α-toxin. *J. Cell Biol.* 91, 83-94.
25. Gouaux, J.E., *et al.*, & Bayley, H. (1994). Subunit stoichiometry of staphylococcal α-hemolysin in crystals and on membranes: a heptameric transmembrane pore. *Proc. Natl Acad. Sci. USA* 91, 12828-12831.
26. Gouaux, E., Hobaugh, M. & Song, L. (1997). α-Hemolysin, γ-hemolysin, and leukocidin from *Staphylococcus aureus*: distant in sequence but similar in structure. *Protein Sci.* 12, 2631-2635.

27. Richardson, J.S. (1981). The anatomy and taxonomy of protein structure. *Adv. Protein Chem.* 34, 167-339.
28. Ward, R.J., Palmer, M., Leonard, K. & Bhakdi, S. (1994). Identification of a putative membrane-inserted segment in the α-toxin of *Staphylococcus aureus*. *Biochemistry* 33, 7477-7484.
29. Valeva, A., Palmer, M., Hilgert, K., Kehoe, M. & Bhakdi, S. (1995). Correct oligomerization is a prerequisite for insertion of the central molecular domain of staphylococcal alpha-toxin into the lipid bilayer. *Biochim. Biophys. Acta* 1236, 213-218.
30. Walker, B., Krishnasastry, M., Zorn, L. & Bayley, H. (1992). Assembly of the oligomeric membrane pore formed by Staphylococcal α-hemolysin examined by truncation mutagenesis. *J. Biol. Chem.* 267, 21782-21786.
31. Valeva, A., Palmer, M. & Bhakdi, S. (1997). Staphylococcal α-toxin: formation of the heptameric pore is partially cooperative and proceeds through multiple intermediate stages. *Biochemistry* 36, 13298-13304.
32. Vécsey-Semjén, B., Lesieur, C., Möllby, R. & van der Goot, F.G. (1997). Conformational changes due to membrane binding and channel formation by staphylococcal α-toxin. *J. Biol. Chem* 272, 5709-5717.
33. Holm, L. & Sander, C. (1993). Protein structure comparison by alignment of distance matrices. *J. Mol. Biol.* 233, 123-138.
34. Kleywegt, G.J. & Jones, T.A. (1994). Halloween... Masks and Bones. In *Proceedings of the CCP4 Study Weekend: From First Map to Final Model* (Bailey, S., Hubbard, R. & Waller, D., eds), pp. 59-66, SERC, Daresbury Laboratory, Warrington, UK.
35. Corfield, P.W., Lee, T.J. & Low, B.W. (1989). The crystal structure of erabutoxin a at 2.0-Å resolution. *J. Biol. Chem.* 264, 9239-9242.
36. Bilwes, A., Rees, B., Moras, D., Ménez, R. & Ménez, A. (1994). X-ray structure at 1.55 Å of toxin γ, a cardiotoxin from *Naja nigricollis* venom. Crystal packing reveals a model for insertion into membranes. *J. Mol. Biol.* 239, 122-136.
37. Rees, B. & Bilwes, A. (1993). Three-dimensional structures of neurotoxins and cardiotoxins. *Chem. Res. Toxicol.* 6, 385-406.
38. Gouaux, E. (1998). α-Hemolysin from *Staphylococcus aureus*: an archetype of β-barrel, channel-forming toxins. *J. Struct. Biol.* 121, 110-122.
39. Cheley, S., *et al*., & Bayley, H. (1997). Spontaneous oligomerization of a staphylococcal α-hemolysin conformationally constrained by removal of residues that form the transmembrane β-barrel. *Protein Eng.* 10, 1433-1443.
40. Murzin, A.G., Lesk, A.M. & Chothia, C. (1994). Principles determining the structure of β-sheet barrels in proteins. I. A theoretical analysis. *J. Mol. Biol.* 236, 1369-1381.
41. Sansom, M.S. & Kerr, I.D. (1995). Transbilayer pores formed by β-barrels: molecular modeling of pore structures and properties. *Biophys. J.* 69, 1334-1343.
42. Colin, D.A., Meunier, O., Staali, L., Prévost, G. & Monteil, H. (1997). Bi-component leukotoxins from *Staphylococcus aureus*. In *Cold Spring Harbor Laboratory on Microbial Pathogenesis and Host Response.* (Maloy, S., Taylor, R.K. & Magee, P.T., eds), pp. 150, Cold Spring Harbor, New York.
43. Czajkowsky, D.M., Sheng, S. & Shao, Z. (1998). Staphylococcal α-hemolysin can form hexamers in phospholipid bilayers. *J. Mol. Biol.* 276, 325-330.
44. Otwinowski, Z. (1993). Oscillation data reduction program. In *Proceedings of the CCP4 Study Weekend: Data Collection and Processing.* (Sawyer, L., Isaccs, N. & Bailey, S., eds), pp. 56-62, SERC, Daresbury Laboratory, Warrington, UK.
45. *Collaborative Computational Project No. 4.* (1994). The CCP4 suite: programs for protein crystallography. *Acta Crystallogr. D* 50, 760-763.
46. de La Fortelle, É. & Bricogne, G. (1997). Maximum-likelihood heavy-atom parameter refinement for multiple isomorphous replacement and multiwavelength anomalous diffraction methods. *Methods Enzymol.* 276, 472-494.
47. Abrahams, J.P. & Leslie, A.G.W. (1996). Methods used in the structure determination of bovine mitochondrial $F_1$ ATPase. *Acta Crystallogr. D* 52, 30-42.
48. Murshudov, G.N., Vagin, A.A. & Dodson, E.J. (1997). Refinement of macromolecular structures by the maximum-likelihood method. *Acta Crystallogr. D* 53, 240-255.
49. Brünger, A.T. (1992). *X-PLOR Version 3.1*. A system for X-ray crystallography and NMR. Yale University Press, New Haven, CT.
50 Roussel, A. & Cambillau, C. (1989). TURBO-FRODO. In *Silicon Graphics Geometry Partner Directory.* pp. 71–78, Silicon Graphics, Mountain View, CA.
51. Brünger, A.T. (1992). The free R value: a novel statistical quantity for assessing the accuracy of crystal structures. *Nature* 355, 472-475.
52. Kraulis, P.J. (1991). MOLSCRIPT: a program to produce both detailed and schematic plots of protein structures. *J. Appl. Crystallogr.* 24, 946-950.
53. Kabsch, W. & Sander, C. (1983). Dictionary of protein secondary structure: pattern recognition of hydrogen-bonded and geometrical features. *Biopolymers* 22, 2577-2637.